Stiffness Modelling of Parallel Mechanisms at Limb and Joint/Link Levels

Haitao Liu, *Member*, *IEEE*, Tian Huang, Derek G. Chetwynd, Andrés Kecskeméthy

***Abstract*—Drawing on screw theory and the virtual joint method, this paper presents a general and hierarchical approach for semi-analytical stiffness modelling of parallel mechanisms. The stiffness model is built by two essential steps: (1) formulating the map between the stiffness matrices of platform and limbs using the duality of wrench and twist of the platform; (2) formulating the map between stiffness matrices of a limb and a number of elastic elements in that limb using the duality of the wrench attributed to the limb and the twist of the end-link of that limb. By merging these two threads, the Cartesian stiffness matrix can be explicitly expressed in terms of the compliance matrices of joints and links. The proposed approach bridges the gap between two currently available approaches, and is thereby very useful for evaluating stiffness over the entire workspace and investigating the influences of joint/link compliances on those of the platform in a quick and precise manner. A stiffness analysis for a 3-PRS parallel mechanism is presented as an example to illustrate the effectiveness of the proposed approach.**

***Index Terms*—Parallel mechanisms, Stiffness modelling, Screw theory**

I. Introduction

Parallel mechanisms have drawn strong interest from academia and industry by offering potential advantages over serial manipulators in terms of better accuracy, higher rigidity and superior dynamics. Stiffness should always be considered and is a particularly important performance factor in the circumstances where high rigidity and fast dynamic response are crucially required for high-speed machining and/or forced assembling applications.

Based upon the combination of fundamental robotics with FEA (Finite Element Analysis) or structural mechanics analytical or semi-analysis stiffness modelling is an essential step in the design flow. The relevant methods have been developed along one of two tracks as follows.

Models developed along the first track establish the relationship between stiffness matrices of the platform and the limbs. The early work was initiated by Salisbury [1] for serial manipulators. Gosselin extended this work to deal with parallel mechanisms by taking into account only actuator compliances [2]. Building upon screw theory [3], [4], Joshi and Tsai [5] developed a general and systematic approach for Jacobian analysis of lower mobility parallel mechanisms, resulting in a brand new Jacobian known as the overall Jacobian, which accounts for the wrenches of both actuations and constraints imposed upon the platform. By utilizing the duality of wrench and twist at the platform, this approach was then substantially extended by Huang and colleagues into the generalized Jacobian [6] that allows the potential integration into a unified framework of velocity, accuracy, and stiffness modelling of lower mobility parallel mechanisms. Under the umbrella of the overall Jacobian or generalized Jacobian, stiffness analyses of a number of lower mobility parallel mechanisms were carried out [7]–[14]. However, the map between stiffness matrices of a limb and links/joints in the joint space has to be obtained by case-by-case studies.

Modelling along the second track develops stiffness models by establishing the relationship between stiffness matrices of the platform and joints/links. The early work was initiated by Zhang and Gosselin [15] who introduced the concept of the 'virtual joint' to express the bending and torsional compliance of a properly constrained passive limb within the Tricept robot, resulting in a simplified bending stiffness model represented by two one-dimensional lumped springs. This elegant idea was then widely used by others [16]–[22]. In order to uniquely determine the location of virtual joints and to fully address the coupling effects, the 'virtual joint' approach was significantly improved by Pashkevich and colleagues [23]–[25]. Their multi-dimensional lumped-parameter model presents the joints/links as pseudo-rigid bodies having 6-DOF virtual springs. Stiffness coefficients of virtual joints can be either roughly evaluated using a regular spatial beam or precisely identified by FEA [23], [26] where the sensibility analysis with respect to the mesh quality is investigated to ensure confidence of the results, allowing sufficient computational accuracy to be achieved. More recently, this approach was used to investigate stiffness modelling of perfect and non-perfect spatial parallel mechanisms under internal and external loadings [27]. Although a general joint-level stiffness model can be achieved by this method, intensive computational efforts have to be

This work is partially supported by the National Natural Science Foundation of China (NSFC) under grants 51622508 and 51420105007, and EU H2020-MSCA-RISE 2016 (734272).

H. Liu is with School of Mechanical Engineering, Tianjin University, Tianjin 300072, China (e-mail: liuht@tju.edu.cn).

T. Huang is with School of Mechanical Engineering, Tianjin University, Tianjin 300072, China (phone: +86 22 27405280; fax: +86 22 27405280; e-mail: tianhuang@tju.edu.cn). He is also partially with the University of Warwick, Coventry CV4 7AL, UK. (e-mail: tian.huang@ warwick.ac.uk)

D. G. Chetwynd is with School of Engineering, University of Warwick, Coventry CV4 7AL, UK. (e-mail: D.G.Chetwynd@warwick.ac.uk).

A. Kecskeméthy is with Chair of Mechanics and Robotics, University of Duisburg-Essen, Duisburg 47057, Germany (e-mail: andres.kecskemethy@ uni-due.de)

made because the Jacobians with respect to passive and virtual joints must be generated by SVD decomposition [25].

To address the practical need for rapid and precise stiffness prediction over entire workspace, this paper offers a new and hierarchical stiffness modelling approach for parallel mechanisms. Following this introduction, the stiffness map between platform and limbs is developed in Section II, using the duality of wrench and twist of the platform. Then, in Section III, the stiffness map in joint space between a limb and elastic elements is formulated using the duality of the wrench attributed to the limb and the twist of the end-link (the platform). By merging these threads in Section IV, a general yet explicit stiffness map between platform and elastic elements is obtained. The stiffness analysis of a 3-PRS parallel manipulator is carried out as an example to illustrate the effectiveness of the proposed approach in Section V, before conclusions are drawn in Section VI. It is worthwhile pointing out that the formulation of the symmetrical component of the Cartesian stiffness matrix is of interest here for design purpose [23] by neglecting the effects caused by the external loads and relevant changes in the Jacobian [28], [29].

II. Stiffness Modelling of Parallel Mechanisms at Limb Level

The first step in the modelling process is to formulate the stiffness model at limb level by screw theory and the virtual work principle. Without loss of generality, consider a parallel mechanism comprising a base, a platform and l limbs as shown in Fig. 1. Assume that there are n_i ($n_i \le 6$) 1-DOF joints in limb i, of which g_i ($0 \le g_i < n_i$) are actuated. For convenience, attach a global reference frame $\mathcal{K}$ to the base and a parallel reference frame $\mathcal{K}'$ to the platform with its three orthogonal axes being parallel to those of $\mathcal{K}$ as depicted in Fig. 1. Note that the coordinates of all vectors are evaluated in $\mathcal{K}'$ unless stated otherwise. Leaving aside gravitational and inertial forces, the externally applied wrench $\$_w$ (expressed in ray-coordinates) imposed upon the platform is equilibrated by the sum of wrenches $\$_{w,i}$ ($i = 1,\ldots,l$) provided by all limbs as shown in Fig. 2.

$$\$_w = \sum_{i=1}^{l} \$_{w,i} = \sum_{i=1}^{l} \boldsymbol{W}_i \bar{\boldsymbol{\rho}}_{w,i} = \boldsymbol{W} \bar{\boldsymbol{\rho}}_w \tag{1}$$

$$\$_{w,i} = \sum_{k=1}^{g_i} \bar{\rho}_{wa,k,i} \hat{\$}_{wa,k,i} + \sum_{j=1}^{6-n_i} \bar{\rho}_{wc,j,i} \hat{\$}_{wc,j,i} = \boldsymbol{W}_i \bar{\boldsymbol{\rho}}_{w,i}, \ i = 1,\ldots,l \tag{2}$$

$$\boldsymbol{W} = \begin{bmatrix} \boldsymbol{W}_1 & \boldsymbol{W}_2 & \cdots & \boldsymbol{W}_l \end{bmatrix}, \ \bar{\boldsymbol{\rho}}_w = \begin{pmatrix} \bar{\boldsymbol{\rho}}_{w,1}^{\mathrm{T}} & \bar{\boldsymbol{\rho}}_{w,2}^{\mathrm{T}} & \cdots & \bar{\boldsymbol{\rho}}_{w,l}^{\mathrm{T}} \end{pmatrix}^{\mathrm{T}}$$

$$\boldsymbol{W}_i = \begin{bmatrix} \hat{\$}_{wa,1,i} & \cdots & \hat{\$}_{wa,g_i,i} & \hat{\$}_{wc,1,i} & \cdots & \hat{\$}_{wc,6-n_i,i} \end{bmatrix}$$

$$\bar{\boldsymbol{\rho}}_{w,i} = \begin{pmatrix} \bar{\rho}_{wa,1,i} & \cdots & \bar{\rho}_{wa,g_i,i} & \bar{\rho}_{wc,1,i} & \cdots & \bar{\rho}_{wc,6-n_i,i} \end{pmatrix}^{\mathrm{T}}$$

where $\hat{\$}_{wa,k,i}$ ($\hat{\$}_{wc,j,i}$) is the kth (jth) unit wrench of actuations (constraints) of limb i with $\bar{\rho}_{wa,k,i}$ ($\bar{\rho}_{wc,j,i}$) being the corresponding intensity. Here, we define a point on the axis of a wrench provided by limb i as being at the interface between the limb and the platform. Then, vector $\bar{\boldsymbol{\rho}}_{w,i}$ collects the generalized reaction forces at the interface. The method for determining the unit wrenches of actuations and constraints of a serial kinematic chain can be found in [30]. Define, also, vector $\bar{\boldsymbol{\rho}}_{t,i}$ (the same size as $\bar{\boldsymbol{\rho}}_{w,i}$) to represent the corresponding interface deflections caused by $\bar{\boldsymbol{\rho}}_{w,i}$. The virtual work principle states that the instantaneous work delivered by the externally applied wrench $\$_w$ on the deflection twist $\$_t$ (expressed in axis-coordinates) of the platform equals the sum of the instantaneous work done by all $\bar{\boldsymbol{\rho}}_{w,i}$ on $\bar{\boldsymbol{\rho}}_{t,i}$, i.e.

$$\$_w^{\mathrm{T}} \$_t = \bar{\boldsymbol{\rho}}_w^{\mathrm{T}} \bar{\boldsymbol{\rho}}_t = \sum_{i=1}^{l} \bar{\boldsymbol{\rho}}_{w,i}^{\mathrm{T}} \bar{\boldsymbol{\rho}}_{t,i} \tag{3}$$

$$\bar{\boldsymbol{\rho}}_t = \begin{pmatrix} \bar{\boldsymbol{\rho}}_{t,1}^{\mathrm{T}} & \bar{\boldsymbol{\rho}}_{t,2}^{\mathrm{T}} & \cdots & \bar{\boldsymbol{\rho}}_{t,l}^{\mathrm{T}} \end{pmatrix}^{\mathrm{T}}$$

$$\bar{\boldsymbol{\rho}}_{t,i} = \begin{pmatrix} \bar{\rho}_{ta,1,i} & \cdots & \bar{\rho}_{ta,g_i,i} & \bar{\rho}_{tc,1,i} & \cdots & \bar{\rho}_{tc,6-n_i,i} \end{pmatrix}^{\mathrm{T}}$$

Substituting (1) into (3) results in

$$\boldsymbol{W}^{\mathrm{T}} \$_t = \bar{\boldsymbol{\rho}}_t \tag{4}$$

or, for each limb

$$\boldsymbol{W}_i^{\mathrm{T}} \$_t = \bar{\boldsymbol{\rho}}_{t,i}, \ i = 1,\ldots,l \tag{5}$$

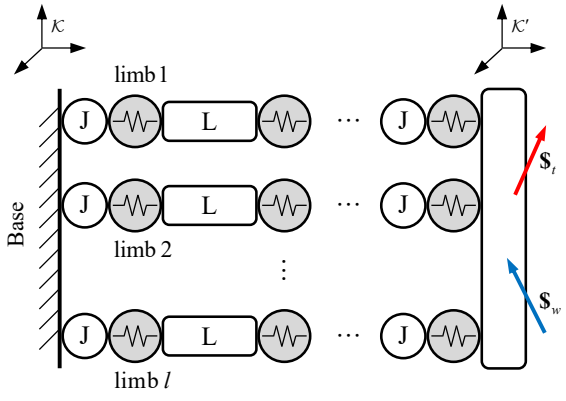

Fig. 1 Elastic model of a parallel mechanism

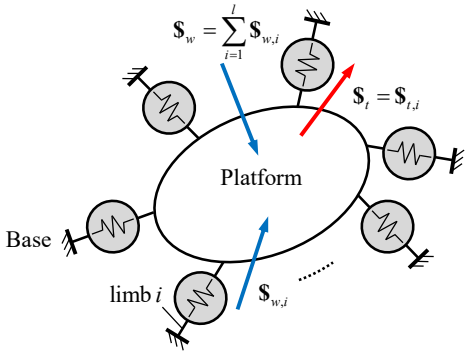

Fig. 2 Static equilibrium of the platform

Assuming that the system is linearly elastic in nature, Hooke's law gives

$$\bar{\boldsymbol{\rho}}_{w,i} = \bar{\boldsymbol{K}}_i \bar{\boldsymbol{\rho}}_{t,i} \text{ or } \bar{\boldsymbol{\rho}}_w = \bar{\boldsymbol{K}}\,\bar{\boldsymbol{\rho}}_t \ , \ \bar{\boldsymbol{K}} = \mathrm{diag}\left[\bar{\boldsymbol{K}}_i\right] \tag{6}$$

where $\bar{\boldsymbol{K}}_i$ is a $(g_i + 6 - n_i)\times(g_i + 6 - n_i)$ symmetrical matrix known as the interface stiffness matrix of limb i with respect to $\mathcal{K}'$. Substituting (4) and (6) into (1) yields the stiffness model at limb level for parallel mechanisms,

$$\$_w = \boldsymbol{K}\$_t \,,\ \boldsymbol{K} = \boldsymbol{W}\bar{\boldsymbol{K}}\boldsymbol{W}^{\mathrm{T}} = \sum_{i=1}^{l} \boldsymbol{W}_i \bar{\boldsymbol{K}}_i \boldsymbol{W}_i^{\mathrm{T}} \tag{7}$$

where $\boldsymbol{K}$ is a 6×6 symmetrical matrix known as the Cartesian stiffness matrix. It is easy to see that $\boldsymbol{K}$ has a structure of l parallel connected springs.

III. Stiffness Map between a Limb and Links/Joints in that Limb in Joint Space

We now develop a method for obtaining a general and explicit expression of $\bar{\boldsymbol{K}}_i$ in terms of stiffness matrices of elastic elements defined in a set of local body-fixed frames. The elastic model of the limb, shown in Fig. 3, comprises $M_i \geq n_i$ elastic elements, each being either a link or 1-DOF revolute or prismatic joint. The choice of a suitable value for M_i depends on the fidelity required.

To evaluate compliances of element m ($m = 1,\ldots,M_i$), attach a body fixed frame $\mathcal{K}_{m,i}$ to the element as shown in Fig. 3, with one axis of $\mathcal{K}_{m,i}$ aligned along the relevant joint axis or along the longitudinal axis of a link. Since all links and joints are being considered as elastic elements, limb i can be visualized as an elastic system comprising M_i serially connected springs as shown in Fig.4. Hence, the deflection twist $\$_{t,i}$ of the end-link of limb i under action of $\$_{w,i}$ can be decomposed into two components as

$$\$_{t,i} = \$^e_{t,i} + \$^d_{t,i} \,,\ i = 1,\ldots,l \tag{8}$$

where $\$^e_{t,i}$ represents the elastic deflections while $\$^d_{t,i}$ arises from the combined rigid body motions of all passive joints in the limb necessary to satisfy the geometric compatibility conditions among the limbs when all elastic elements and actuated joints are locked. $\$^d_{t,i}$ can be further parameterized as a linear combination of a set of unit twists associated with all the passive joints involved,

$$\$^d_{t,i} = \sum_{p=1}^{n_i - g_i} \rho_{ta,p,i}\,\hat{\$}_{ta,p,i} \tag{9}$$

where $\hat{\$}_{ta,p,i}$ denotes the unit twist due to the translation along and rotation about the pth passive joint axis with $\rho_{ta,p,i}$ being the associated amplitude. All limbs connect to the same platform and share its motion, i.e., $\$_t = \$_{t,i}$, and therefore $\hat{\$}_{wa,k,i}$ ($k = 1,\ldots,g_i$) and $\hat{\$}_{wc,j,i}$ ($j = 1,\ldots,6-n_i$) must be reciprocal to $\hat{\$}_{ta,p,i}$ ($p = 1,\ldots,n_i - g_i$) because $\$_{w,i}$ does work only on $\$^e_{t,i}$ but not on $\$^d_{t,i}$ [6]. These dual and reciprocal properties lead to the relationships

$$\boldsymbol{W}_i^{\mathrm{T}}\$_t = \boldsymbol{W}_i^{\mathrm{T}}\$_{t,i} = \boldsymbol{W}_i^{\mathrm{T}}\$^e_{t,i} = \bar{\boldsymbol{\rho}}_{t,i} \,,\ \boldsymbol{W}_i^{\mathrm{T}}\$^d_{t,i} = 0 \tag{10}$$

In addition, because all the elastic elements are connected serially as shown in Fig. 4, $\$^e_{t,i}$ can be written as the sum of their elastic deflection twists $\$^e_{t,m,i}$ ($m = 1,\ldots,M_i$) under the action of $\$_{w,i}$,

$$\$^e_{t,i} = \sum_{m=1}^{M_i} \$^e_{t,m,i} \,,\ i = 1,\ldots,l \tag{11}$$

Consider, first, only elements that are a 1-DOF actuated joint or an elastic link. Let $\boldsymbol{\rho}_{w,m,i}$ be a 6×1 vector collecting the reaction forces/moments along/about the axes of $\mathcal{K}_{m,i}$, and $\boldsymbol{\rho}_{t,m,i}$ be the vector, the same size as $\boldsymbol{\rho}_{w,m,i}$, that represents the elastic deflections caused by $\boldsymbol{\rho}_{w,m,i}$. Then, from Hooke's law

$$\boldsymbol{\rho}_{w,m,i} = \boldsymbol{K}_{m,i}\boldsymbol{\rho}_{t,m,i} \tag{12}$$

where $\boldsymbol{K}_{m,i}$ is $n\times n$ symmetrical matrix defined as the stiffness matrix of element m with respect to $\mathcal{K}_{m,i}$ and for these cases $n = 6$. If, however, the element is a 1-DOF passive joint, this exact formulation cannot be used; the freedom would cause the matrix to be singular and the compliance matrix would not exist. The solution is to use a reduced form of the stiffness matrix with $n = 5$ that covers only the constrained axes, with the corresponding vectors also reduced to 5×1. $\boldsymbol{K}_{m,i}$ can be generated by either FEA or by an $n-$DOF virtual spring that gives diagonal entries.

Let $\boldsymbol{T}_{m,i}$ be the adjoint coordinate transformation matrix of $\mathcal{K}_{m,i}$ with respect to $\mathcal{K}'$. Each column of $\boldsymbol{T}_{m,i}$ should be understood as a unit twist produced by a pure translation/

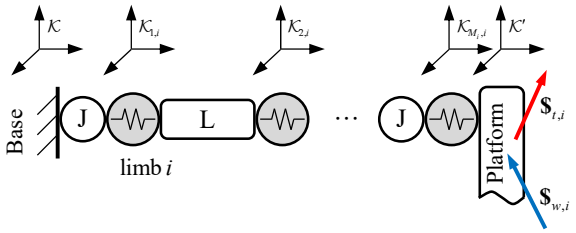

Fig. 3 Flexible model of a limb

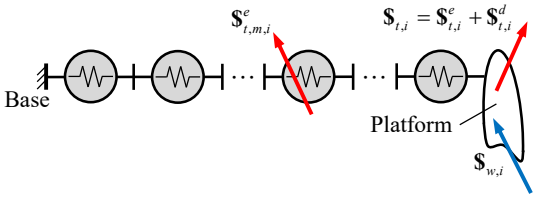

Fig. 4 Equilibrium of serial connected springs

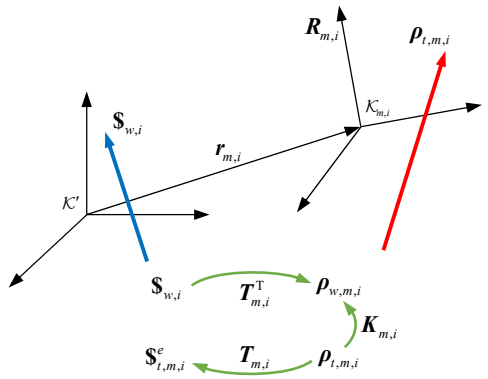

Fig. 5 Coordinate transformation between $\mathcal{K}_{m,i}$ and $\mathcal{K}'$

rotation along/about the corresponding axis of $\mathcal{K}_{m,i}$. Again, considering at first only the cases of 1-DOF actuated joints and elastic links, the principle of virtual work shows that

$$\boldsymbol{\rho}_{w,m,i} = \boldsymbol{T}_{m,i}^{\mathrm{T}} \$_{w,i}\,,\ \$_{t,m,i}^{e} = \boldsymbol{T}_{m,i}\boldsymbol{\rho}_{t,m,i}\,,\ m = 1,\ldots,M_i\,,\ i = 1,\ldots,l \quad (13)$$

For these cases $\boldsymbol{T}_{m,i}$ has the (6×6) form

$$\boldsymbol{T}_{m,i} = \begin{bmatrix} \boldsymbol{R}_{m,i} & \left[\boldsymbol{r}_{m,i}\times\right]\boldsymbol{R}_{m,i} \\ \boldsymbol{0} & \boldsymbol{R}_{m,i} \end{bmatrix} \quad (14)$$

Here, $\boldsymbol{R}_{m,i}$ denotes the orientation matrix of $\mathcal{K}_{m,i}$ with respect to $\mathcal{K}'$ and $\left[\boldsymbol{r}_{m,i}\times\right]$ denotes the skew-symmetric matrix of the vector $\boldsymbol{r}_{m,i}$ pointing from the origin of $\mathcal{K}'$ to that of $\mathcal{K}_{m,i}$ as depicted in Fig.5. For a 1-DOF passive joint, the $\boldsymbol{T}_{m,i}$ given in (14) must be reduced by removing its column corresponding to the unit twist of the rigid body motion along/about the free axis, so giving a 6×5 matrix compatible with the reduced stiffness matrices and vectors proposed above.

Substituting (12) and (13) into (11) yields the stiffness model of serial kinematic chains containing passive joints,

$$\$_{w,i} = \left(\sum_{m=1}^{M_i} \boldsymbol{T}_{m,i}\boldsymbol{K}_{m,i}^{-1}\boldsymbol{T}_{m,i}^{\mathrm{T}}\right)^{-1} \$_{t,i}^{e} \quad (15)$$

Substituting (10) into (15) and left-multiplying both sides by $\boldsymbol{W}_i^{\mathrm{T}}$, yields

$$\bar{\boldsymbol{\rho}}_{w,i} = \left(\boldsymbol{W}_i^{\mathrm{T}}\left(\sum_{m=1}^{M_i} \boldsymbol{T}_{m,i}\boldsymbol{K}_{m,i}^{-1}\boldsymbol{T}_{m,i}^{\mathrm{T}}\right)\boldsymbol{W}_i\right)^{-1} \bar{\boldsymbol{\rho}}_{t,i} \quad (16)$$

Finally, the stiffness map between $\boldsymbol{K}_{m,i}$ and $\bar{\boldsymbol{K}}_i$ is obtained by equating (6) with (16) to give

$$\bar{\boldsymbol{K}}_i = \left(\boldsymbol{W}_i^{\mathrm{T}}\left(\sum_{m=1}^{M_i}\left(\boldsymbol{T}_{m,i}\boldsymbol{K}_{m,i}^{-1}\boldsymbol{T}_{m,i}^{\mathrm{T}}\right)\right)\boldsymbol{W}_i\right)^{-1} \quad (17)$$

Equation (17) can be interpreted as the map between stiffness matrices of limbs and of their elastic elements in joint space according to the convention defined in robotics [4]. Clearly, $\bar{\boldsymbol{K}}_i$ has a structure analogous to that of M_i serially connected springs. This general and explicit derivation of $\bar{\boldsymbol{K}}_i$ by using the dual and reciprocal properties of the relevant wrenches and twists is one major contribution of this article.

IV. Stiffness Modelling of Parallel Mechanisms at the Joint/Link (Element) Level

Having established the results of Sections II and III, the element-level stiffness model for parallel mechanisms is obtained simply by substituting (17) into (7) such that

$$\$_w = \boldsymbol{K}\$_t \quad (18)$$

$$\boldsymbol{K} = \sum_{i=1}^{l} \boldsymbol{W}_i\bar{\boldsymbol{K}}_i\boldsymbol{W}_i^{\mathrm{T}}\,,\ \bar{\boldsymbol{K}}_i = \left(\boldsymbol{W}_i^{\mathrm{T}}\left(\sum_{m=1}^{M_i}\left(\boldsymbol{T}_{m,i}\boldsymbol{K}_{m,i}^{-1}\boldsymbol{T}_{m,i}^{\mathrm{T}}\right)\right)\boldsymbol{W}_i\right)^{-1}$$

Fig. 6 illustrates the hierarchical structure of the stiffness model developed in this article. Closely linked by the explicit expression of the map given in (17), the model is clearly built at two levels, i.e. the limb level given in (7) by using screw theory, and the element level given in (18) by combining screw theory with the virtual joint method.

Hence, the stiffness model of the system as a whole can be formulated by simply taking account also of the elasticity of the platform, to give

$$\boldsymbol{K}_M = \left(\boldsymbol{K}^{-1} + \boldsymbol{K}_{\boldsymbol{p}}^{-1}\right)^{-1}\,,\ \boldsymbol{K}_p = \left(\boldsymbol{T}_p\boldsymbol{K}_{p0}^{-1}\boldsymbol{T}_p^{\mathrm{T}}\right)^{-1} \quad (19)$$

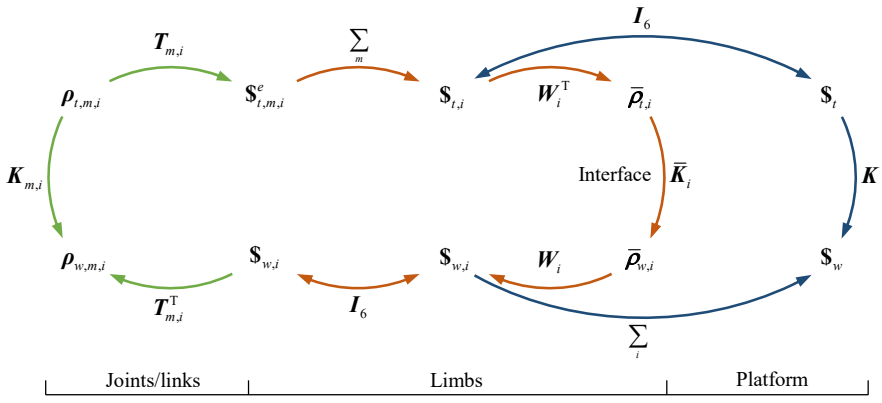

Fig. 6 Hierarchical structure of the stiffness model of parallel mechanisms

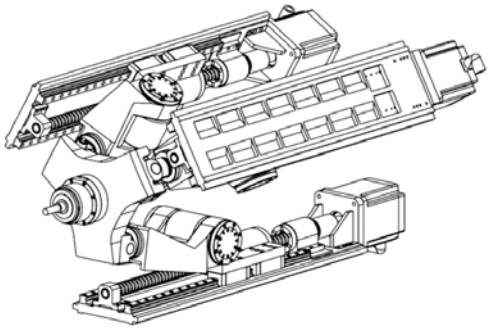

Fig. 7 CAD model of a 3-PRS spindle head

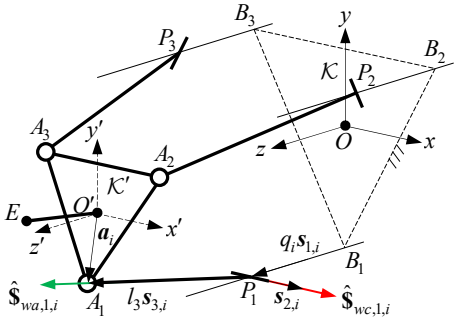

Fig. 8 Schematic diagram of a 3-PRS mechanism

TABLE I
COMPLIANCE MATRICES OF ELASTIC ELEMENTS

m	Element and $\mathcal{K}_{m,i}$	$\boldsymbol{K}_{m,i}^{-1}$ (unit: N, m, rad)
1	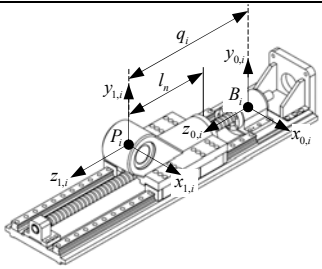	$\begin{bmatrix} 3.39 & 1.72\times10^{-3} & -0.86\times10^{-3} & -5.58\times10^{-3} & 13.92 & -9.18 \\ & 1.47 & -0.91\times10^{-3} & -10.26 & 0.52\times10^{-3} & -29.06\times10^{-3} \\ & & k_{zz,i}^{-1}+1.55 & 9.65 & -5.78 & 1.50 \\ & & & 139.04 & -44.74\times10^{-3} & 102.07\times10^{-3} \\ & \text{sym.} & & & 150.99 & -6.48 \\ & & & & & 143.91 \end{bmatrix}\times10^{-9}$
2	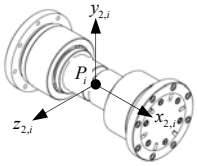	$\begin{bmatrix} 0.73 & -0.21\times10^{-3} & -0.16\times10^{-3} & -1.84\times10^{-3} & -0.22\times10^{-3} \\ & 0.42 & -0.31\times10^{-3} & -6.40\times10^{-3} & -4.66\times10^{-3} \\ & & 0.42 & -13.19\times10^{-3} & 6.40\times10^{-3} \\ & \text{sym.} & & 52.02 & 39.27\times10^{-3} \\ & & & & 52.33 \end{bmatrix}\times10^{-9}$
3	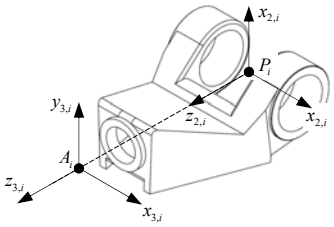	$\begin{bmatrix} 5.17 & -15.05\times10^{-3} & 2.26\times10^{-3} & 64.02\times10^{-3} & 21.85 & -0.37 \\ & 28.29 & -3.74 & -103.28 & -54.45\times10^{-3} & -85.47\times10^{-3} \\ & & 1.03 & 12.94 & -0.63\times10^{-3} & 19.67\times10^{-3} \\ & & & 452.99 & 0.33 & 0.36 \\ & \text{sym.} & & & 170.74 & 27.11 \\ & & & & & 227.72 \end{bmatrix}\times10^{-9}$
4	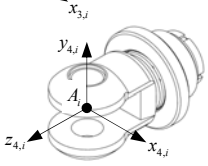	$\begin{bmatrix} 11.97 & -4.19\times10^{-3} & 6.63\times10^{-3} & 45.32\times10^{-3} & 106.97 \\ & 16.25 & 2.07\times10^{-3} & -117.47 & -121.12\times10^{-3} \\ & & 1.04 & -30.50\times10^{-3} & 89.04\times10^{-3} \\ & \text{sym.} & & 141.85 & 1.19 \\ & & & & 182.99 \end{bmatrix}\times10^{-9}$
5	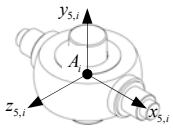	$\begin{bmatrix} 4.09 & -0.17\times10^{-3} & 6.74\times10^{-6} & 4.74\times10^{-3} & 6.72\times10^{-3} \\ & 1.79 & -0.15\times10^{-3} & 64.62\times10^{-3} & -17.29\times10^{-3} \\ & & 4.25 & -12.90\times10^{-3} & -2.42\times10^{-3} \\ & \text{sym.} & & 57.69\times10^{3} & -0.43 \\ & & & & 55.45\times10^{3} \end{bmatrix}\times10^{-9}$
6	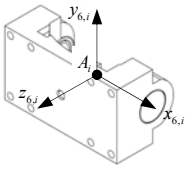	$\begin{bmatrix} 1.14 & -0.41\times10^{-3} & -0.20\times10^{-3} & 18.35\times10^{-3} & 8.96\times10^{-3} \\ & 2.65 & 30.17\times10^{-6} & 18.89\times10^{-6} & 4.08\times10^{-3} \\ & & 2.66 & -14.78\times10^{-3} & 7.79\times10^{-3} \\ & \text{sym.} & & 856.82 & -9.24\times10^{-3} \\ & & & & 874.76 \end{bmatrix}\times10^{-9}$

where $\boldsymbol{K}_{p0}$ is the stiffness matrix of the platform evaluated in its local frame $\mathcal{K}_0$ and $\boldsymbol{T}_p$ is the adjoint coordinate transformation matrix of $\mathcal{K}_0$ with respect to $\mathcal{K}'$, which has a similar form to that given in (14). Note, finally, that because of the coupling effects between translational and rotational components, $\bar{\boldsymbol{K}}_i$ is in general a non-diagonal matrix even when all related $\boldsymbol{K}_{m,i}$ are diagonal matrices as assumed by the virtual joint method.

V. An Example

In this section, a stiffness analysis of a 3-PRS parallel mechanism is carried out to illustrate the generality and effectiveness of the proposed approach. The mechanism can be used to build a 3-DOF spindle head shown in Fig. 7, e.g., the Sprint Z3 head [31]–[33], as part of a 5-axis CNC machine tool for high-speed machining of large structural components in, e.g., the aircraft industry.

Fig. 8 shows a schematic diagram of the 3-PRS parallel mechanism. It comprises a base, a platform, and three identical limbs, each connecting the base with the platform by, in sequence, an actuated prismatic joint P, a revolute joint R, and a spherical joint S. The spherical joint is a composite joint of revolute joint and universal joint. A reference frame $\mathcal{K}$ is attached to the base with O located at the centre of equilateral triangle $\Delta B_1B_2B_3$, its z axis normal to the plane of $\Delta B_1B_2B_3$ and its x axis parallel to $\overline{B_2B_3}$. An instantaneous frame $\mathcal{K}'$ is attached to the platform with O' located at the centre of equilateral triangle $\Delta A_1A_2A_3$, and the x', y' and z' axes parallel to x, y and z, respectively. Then, the unit wrenches in $\boldsymbol{W}_i$ that is defined in (2) can be generated by the method given in [30],

$$\boldsymbol{W}_i = \begin{bmatrix} \hat{\$}_{wa,1,i} & \hat{\$}_{wc,1,i} \end{bmatrix} \tag{20}$$

$$\hat{\$}_{wa,1,i} = \begin{pmatrix} \boldsymbol{s}_{3,i} \\ \boldsymbol{a}_i \times \boldsymbol{s}_{3,i} \end{pmatrix},\ \hat{\$}_{wc,1,i} = \begin{pmatrix} \boldsymbol{s}_{2,i} \\ \boldsymbol{a}_i \times \boldsymbol{s}_{2,i} \end{pmatrix},\ \boldsymbol{s}_{2,i} \perp \boldsymbol{s}_{3,i},\ i = 1,2,3$$

where $\boldsymbol{s}_{2,i}$ is a unit vector of the R joint axis, $\boldsymbol{s}_{3,i}$ is a unit vector aligned with $\overline{P_iA_i}$, and $\boldsymbol{a}_i = \overline{O'A_i}$ as shown in Fig. 8.

For convenience, we group all parts of a PRS limb into six elastic elements shown Table I: (1) the carriage assembly; (2) the R joint; (3) the limb body; (4)-(6) three R joints of the S joint, numbered from the one connecting with the limb body to that with the platform. To evaluate $\boldsymbol{K}_{m,i}^{-1}$, place a reference frame $\mathcal{K}_{0,i}$ at B_i with its $x_{0,i}$ axis parallel to the axis of the R joint and its $z_{0,i}$ axis along the direction of the P joint. Then place $\mathcal{K}_{m,i}$ ($m = 1,2,3$) at P_i with $x_{0,i} \,/\!/\, x_{1,i}$, $x_{1,i} \,/\!/\, x_{2,i}$, $x_{2,i} \,/\!/\, x_{3,i}$, $z_{0,i} \,/\!/\, z_{1,i}$ and $z_{2,i} \,/\!/\, z_{3,i}$; and $\mathcal{K}_{m,i}$ ($m = 4,5,6$) at A_i with $z_{3,i} \,/\!/\, z_{4,i}$, $y_{4,i} \,/\!/\, y_{5,i}$, $x_{5,i} \,/\!/\, x_{6,i}$, respectively. Here, the $z_{2,i}$ axis is aligned with $\overline{P_iA_i}$; the $x_{2,i}$, $z_{4,i}$, $y_{5,i}$ and $x_{6,i}$ axes are aligned with the rotational axes of the four passive R joints. Using these local frames, $\boldsymbol{T}_{m,i}$ ($m = 1,\ldots,6$) can be generated *via* inverse kinematic analysis, with the geometric parameters for this specific example given in Table II [14]. Table I shows $\boldsymbol{K}_{m,i}^{-1}$ obtained with the aid of FEA software SAMCEF® by taking account of compliances of all relevant bearings and mechanical parts, each evaluated in its corresponding local frame $\mathcal{K}_{m,i}$ by taking 'virtual loading experiments' [24], [26]. Data for FEA was taken from manufacturers' specifications and typical materials properties. The only non-constant term here is the compliance coefficient $k_{zz,i}^{-1}$ in $\boldsymbol{K}_{1,i}^{-1}$, where the axial compliance of the lead-screw is a function of stroke q_i. Since the support condition of lead-screw is Fixed-Free support [34], $k_{zz,i}^{-1}$ can be modelled as [14]

TABLE II
Geometric Parameters

$\lVert\overline{O'A_i}\rVert$	$\lVert\overline{OB_i}\rVert$	$\lVert\overline{P_iA_i}\rVert$	$\lVert\overline{O'E}\rVert$
0.170 m	0.220 m	0.390 m	0.238 m

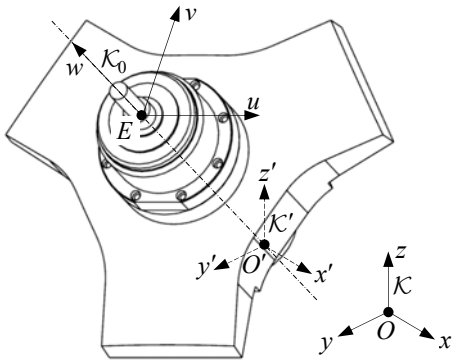

Fig. 9 Body fixed frame at point *E*

$$k_{zz,i}^{-1} = (q_i - l_n)/EA + k_{an}^{-1} + k_{ar}^{-1} \tag{21}$$

where EA is the tensile modulus of the lead-screw, k_{an} and k_{ar} are the extension/compression stiffness coefficients of the nut and rear support bearings, respectively. Values for this example, based on the relevant product specifications, are

$$l_n = 0.318 \text{ m},\ EA = 1.465 \times 10^8 \text{ N}$$

$$k_{an} = 1.104 \times 10^9 \text{ N/m},\ k_{ar} = 2.140 \times 10^9 \text{ N/m}$$

For applications as a machine tool, it is physically meaningful and desirable to evaluate the mechanism rigidity in a body fixed frame $\mathcal{K}_0$ placed at point *E* on the platform with the *u* axis along the direction and the *w* axis aligned with the spindle axis as shown in Fig. 9. Then, the stiffness matrix at point *E* with respect to $\mathcal{K}_0$ can be expressed, from (19), as

$$\boldsymbol{K}_E = \boldsymbol{T}_E^{-\mathrm{T}} \boldsymbol{K}_M \boldsymbol{T}_E^{-1} = \left(\boldsymbol{T}_E \boldsymbol{K}^{-1} \boldsymbol{T}_E^{\mathrm{T}} + \boldsymbol{K}_{p0}^{-1} \right)^{-1} \tag{22}$$

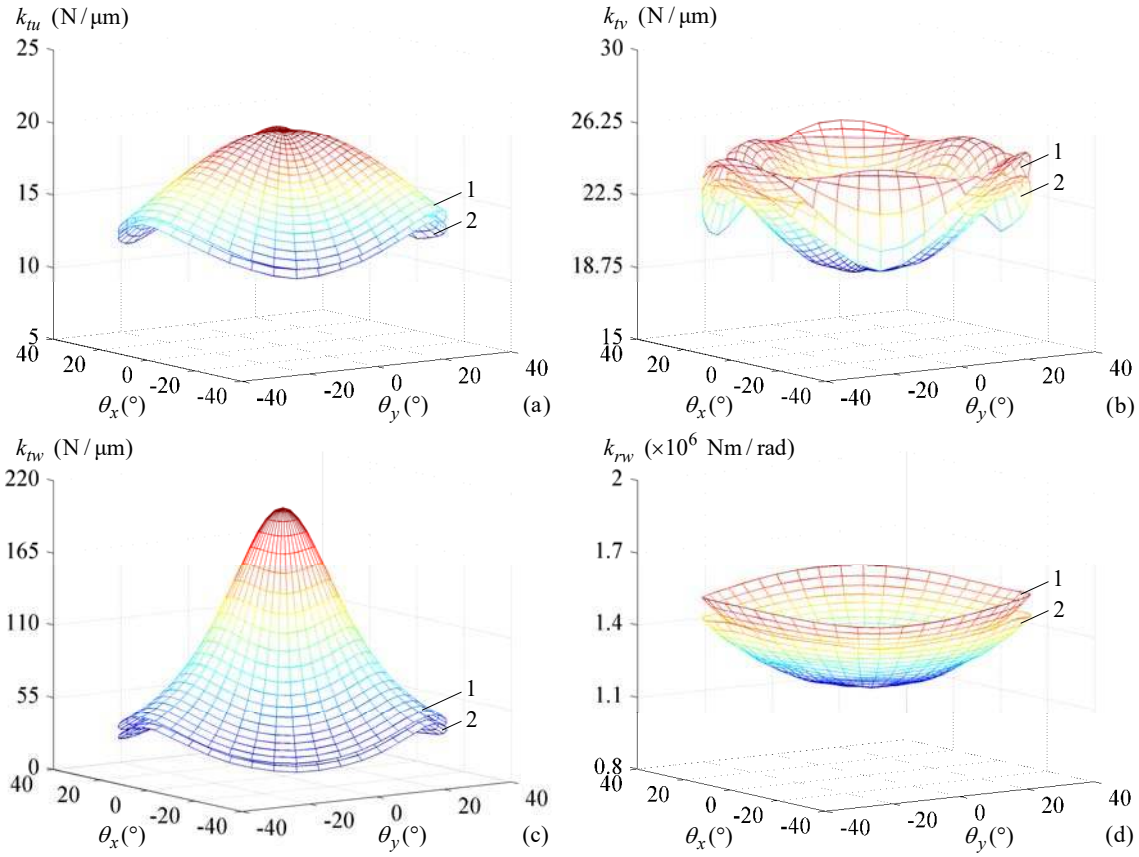

Fig. 10 Stiffness distributions of the 3-PRS parallel mechanism ($\theta_x = \theta\sin\psi$, $\theta_y = -\theta\sin\psi$)

1: Semi-analytical model 2: FEA model

TABLE III
RESULTS OBTAINED BY THE SEMI-ANALYTICAL METHOD AND FEA

	k_{tu} N/μm	k_{tv} N/μm	k_{tw} N/μm	k_{rw} $\times 10^6$ Nm/rad
Semi-Analytic	19.95	19.95	204.46	1.25
FEA	18.97	18.97	198.07	1.18
Residual	5.17%	5.17%	3.23%	5.93%

$$\boldsymbol{T}_E = \begin{bmatrix} \boldsymbol{R}^{\mathrm{T}} & [\boldsymbol{r}_{EO'}\times]\boldsymbol{R}^{\mathrm{T}} \\ \boldsymbol{0} & \boldsymbol{R}^{\mathrm{T}} \end{bmatrix},\quad \boldsymbol{R} = \begin{bmatrix} \cos\psi & -\cos\theta\sin\psi & \sin\theta\sin\psi \\ \sin\psi & \cos\theta\cos\psi & -\sin\theta\cos\psi \\ 0 & \sin\theta & \cos\theta \end{bmatrix}$$

where $\boldsymbol{R}$ is the orientation matrix of $\mathcal{K}_0$ with respect to $\mathcal{K}'$. $\boldsymbol{r}_{EO'} = (0 \quad 0 \quad -e)^{\mathrm{T}}$ is the position of point O' measured in $\mathcal{K}_0$ with e being the distance between point O' and point E. Note that $\boldsymbol{T}_E$ is the inverse transformation of $\boldsymbol{T}_p$. Here,

$$\boldsymbol{K}_{p0}^{-1} = \begin{bmatrix} 0.69 & 0 & 0 & 0 & 4.79 & 0 \\ & 0.68 & 0 & -4.46 & 0 & 0 \\ & & 0.14 & 0 & 0 & 0 \\ & & & 40.42 & 0 & 0 \\ & \text{sym.} & & & 46.64 & 0 \\ & & & & & 23.96 \end{bmatrix} \times 10^{-9}$$

We now use linear stiffnesses along the u, v, w axes and torsional stiffness about the w axis of $\mathcal{K}_0$ to evaluate the rigidities of the mechanism for milling purpose. These rigidities are the reciprocal diagonal entries of $\boldsymbol{C}_E = \boldsymbol{K}_E^{-1}$, i.e.

$$k_{tu} = 1/\boldsymbol{C}_E(1,1),\ k_{tv} = 1/\boldsymbol{C}_E(2,2)$$
$$k_{tw} = 1/\boldsymbol{C}_E(3,3),\ k_{rw} = 1/C_E(6,6)$$

Fig. 10 shows the distributions of k_{tu}, k_{tv}, k_{tw}, and k_{rw} over a portion of the task workspace defined by the precession angle $\psi = 0^\circ \sim 360^\circ$, the nutation angle $\theta = 0^\circ \sim 40^\circ$, and the fixed coordinate $z = 1.055$ m. The results are obtained respectively by the semi-analytical model given in (22) and by SAMCEF® FEA software. In the FEA implementation, the translational displacements along three orthogonal axes of $\mathcal{K}_0$ and the angular displacement about the w axis of $\mathcal{K}_0$ under unit force and unit torque are evaluated at each configuration (a pair of ψ and θ), respectively. Then, at a given configuration, k_{tu}, k_{tv}, k_{tw}, and k_{rw} are obtained by taking reciprocal of the relevant linear and angular displacements. Table III compares the results at the specific configuration where $z = 1.055$ m, $\psi = 0^\circ$, and $\theta = 0^\circ$. The results obtained by the proposed approach clearly match satisfactorily those obtained by FEA in terms of both magnitude and distribution. Given this full

confidence in terms of its computational accuracy, the proposed semi-analytical approach offers a great benefit over FEA: a huge computational time can be saved when predicting the stiffness over the entire workspace, an important issue in the conceptual as well as the joint-level mechanical design of a parallel mechanism.

VI. Conclusions

By combining screw theory with the virtual joint method, this paper introduces a general and systematic approach for stiffness modelling of parallel mechanisms under 'unloaded equilibrium' conditions. The following conclusions are drawn.

(1) We have proposed a hierarchical structure of the stiffness model of parallel mechanisms that essentially consists of two stiffness maps: (a) the map between stiffness matrices in the Cartesian space and in the joint space at limb level, which has the nature of a system comprising a set of parallel connected spring elements; (b) the map between stiffness matrices in the joint space at limb level and at element level, which has the nature of a set of serially connected springs. Merging these two threads results in a general, explicit expression for the Cartesian stiffness matrix in terms of the compliance matrices of all joints/links evaluated in their local body-fixed frames, the wrench systems imposed upon the limbs, and the twist systems generated by the virtual joints.

(2) The effectiveness of the proposed approach has been confirmed by a comparison study against FEA software. The results of a stiffness analysis of a 3-DOF spindle head show that sufficient computational accuracy can be achieved while making huge computational time savings (over FEA) for the prediction of stiffness over the entire workspace. The proposed approach is therefore valuable in both the conceptual design and element-level optimization of parallel mechanisms, including those having kinematic redundancy and over-constraints.

References

[1] J. Salisbury, "Active stiffness control of a manipulator in Cartesian coordinates," in *19th IEEE Conf. Dec. Control*, 1980, pp. 87–97.

[2] C. M. Gosselin, "Stiffness mapping for parallel manipulators," *IEEE Trans. on Robot. Autom.*, vol. 6, no. 3, pp. 377–382, 1990.

[3] K. H. Hunt, *Kinematic Geometry of Mechanisms*. Oxford University Press, 1978.

[4] L. W. Tsai, *Robot analysis: the mechanics of serial and parallel manipulators*. New York: John Wiley & Sons Inc., 1999.

[5] S. Joshi and L. W. Tsai, "Jacobian analysis of limited-DOF parallel manipulators," *ASME J. Mech. Des.*, vol. 124, no. 2, pp. 254–258, 2002.

[6] T. Huang, H. T. Liu, and D. G. Chetwynd, "Generalized Jacobian analysis of lower mobility manipulators," *Mech. Mach. Theory*, vol. 46, no. 5, pp. 831–844, 2011.

[7] M. Zoppi, D. Zlatanov, and R. Molfino, "On the velocity analysis of interconnected chains mechanisms," *Mech. Mach. Theory*, vol. 41, no. 11, pp. 1346–1358, 2006.

[8] Y. M. Li and Q. S. Xu, "Kinematics and stiffness analysis for a general 3-PRS spatial parallel mechanism," in *Proc. IFToMM Symp. Rob. Des. Dyn.*, Montreal, Canada, 2004.

[9] J. W. Kim, K. W. Kim, H. S. Kim, and J. H. Kyung, "Stiffness analysis and design of a 3-DOF parallel robot with one constraining leg," in *Proc. Int. Conf. Control, Autom. Sys.*, Seoul, Korea, 2007, pp. 2288–2293.

[10] Q. S. Xu and Y. M. Li, "An investigation on mobility and stiffness of a 3-DOF translational parallel manipulator via screw theory," *Robot. Computer-Integrated Manuf.*, vol. 24, no. 3, pp. 402–414, 2008.

[11] Y. M. Li and Q. S. Xu, "Stiffness analysis for a 3-PUU parallel kinematic machine," *Mech. Mach. Theory*, vol. 43, no. 2, pp. 186–200, 2008.

[12] M. B. Hong and Y. J. Choi, "Kinestatic analysis of nonsingular lower mobility manipulators," *IEEE Trans. Robot.*, vol. 25, no. 4, pp. 938–942, 2009.

[13] Y. Y. Wang, H. T. Liu, T. Huang, and D. G. Chetwynd, "Stiffness modelling of the Tricept robot using the overall Jacobian matrix," *ASME J. Mech. Robot.*, vol. 1, no. 2, pp. 021002.1–021002.8, 2009.

[14] Y. G. Li , H. T. Liu, X. M. Zhao, T. Huang, and D. G. Chetwynd, "Design of a 3-DOF PKM module for large structural component machining," *Mech. Mach. Theory*, vol. 45, no. 6, pp. 941–954, 2010.

[15] D. Zhang and C. M. Gosselin, "Kinetostatic modelling of N-DOF parallel mechanisms with a passive constraining leg and prismatic actuators," *ASME J. Mech. Des.*, vol. 123, no. 9, pp. 375–381, 2001.

[16] C. M. Gosselin and D. Zhang, "Stiffness analysis of parallel mechanisms using a lumped model," *Int. J. Robot. Autom.*, vol. 17, no. 1, pp. 17–27, 2002.

[17] D. Zhang and C. M. Gosselin, "Kinetostatic modelling of parallel mechanisms with a passive constraining leg and revolute actuators," *Mech. Mach. Theory*, vol. 37, pp. 599–617, 2002.

[18] D. Zhang and C. M. Gosselin, "Kinetostatic analysis and design optimization of the Tricept machine tool family," *ASME J. Manuf. Sci. Eng.*, vol. 124, no. 3, pp. 725–733, 2002.

[19] D. Zhang, F. Xi, C. M. Gosselin, and S. Y. T. Lang, "Analysis of parallel kinematic machine with kinetostatic modelling method," *Robot. Computer-Integrated Manuf.*, vol. 20, no. 2, pp. 151–165, 2004.

[20] D. Zhang and S. Y. T. Lang, "Stiffness modelling for a class of reconfigurable PKMs with three to five degrees of freedom," *J. Manuf. Sys.*, vol. 23, no. 4, pp. 316–327, 2004.

[21] D. Zhang and L. Wang, "Conceptual development of an enhanced tripod mechanism for machine tool," *Robot. Computer-Integrated Manuf.*, vol. 21, no. 4-5, pp. 318–327, 2005.

[22] D. Zhang, Z. M. Bi, and B. Z. Li, "Design and kinetostatic analysis of a new parallel manipulator," *Robot. Computer-Integrated Manuf.*, vol. 25, no. 4-5, pp. 782–791, 2009.

[23] A. Pashkevich, D. Chablat, and P. Wenger, "Stiffness analysis of over-constrained parallel manipulators," *Mech. Mach. Theory*, vol. 44, no. 5, pp. 966–982, 2009.

[24] A. Pashkevich, A. Klimchik, and D. Chablat, "Enhanced stiffness modeling of manipulators with passive joints," *Mech. Mach. Theory*, vol. 46, no. 5, pp. 662–679, 2011.

[25] A. Klimchik, A. Pashkevich, S. Caro, and D. Chablat, "Stiffness matrix of manipulators with passive joints: computational aspects," *IEEE Trans. Robot.*, vol. 28, no. 4, pp. 954–958, 2012.

[26] A. Klimchik, A. Pashkevich, and D. Chablat, "CAD-based approach for identification of elasto-static parameters of robotic manipulators," *Finite Elem. Anal. Des.*, vol. 75, pp. 19–30, 2013.

[27] A. Klimchik, D. Chablat, A. Pashkevich, "Stiffness modeling for perfect and non-perfect parallel manipulators under internal and external loadings," *Mech. Mach. Theory*, vol. 75, pp. 1–28, 2014.

[28] S. F. Chen and I. Kao, "Conservative congruence transformation for joint and Cartesian stiffness matrices of robotic hands and fingers," *Int. Robot. Research*, vol. 19, no. 9, pp. 835–847, 2000.

[29] S. F. Chen, "The 6× 6 stiffness formulation and transformation of serial manipulators via the CCT theory," in *Proc. IEEE Int. Conf. Robot. Autom.*, Taipei, Taiwan, 2003, pp. 4042-4047.

[30] T. Huang, S. F. Yang, M. X. Wang, T. Sun, and D. G. Chetwynd, "An approach to determining the unknown twist/wrench subspaces of lower mobility serial kinematic chains," *ASME J. Mech. Robot.*, vol. 7, no. 3, pp. 031003.1–031003.9, 2015.

[31] H. Hennes, "Ecospeed: an innovative machining concept for high performance 5-axis-machining of large structural component in aircraft engineering," in Proc. 3rd Chemnitz Parallel kinematics Seminar, Chemnitz, Germany, 2002, pp. 763–774.

[32] Y. M. Li and Q. Xu, "Kinematic Analysis of a 3-PRS Parallel Manipulator," *Rob. Computer-Integrated Manuf.*, vol. 23, no. 4, pp. 395–408, 2007.

[33] Y. M. Li and Q. Xu, "Kinematics and Inverse Dynamics Analysis for a General 3-PRS Parallel Mechanism," *Robotica*, vol. 23, no. 2, pp. 219–229, 2005.

[34] J.-S. Chen and W.-Y. Hsu, "Design and analysis of a tripod machine tool with an integrated Cartesian guiding and metrology mechanism," *Precision Engineering*, vol. 28, no. 1, pp. 46–57, 2004.